Sparse Estimation of Light Transport Matrix under Saturated Condition

Naoya Chiba
chiba@ic.is.tohoku.ac.jp
Koichi Hashimoto
koichi@tohoku.ac.jp

Department of System Information Sciences, Graduate School of Information Sciences
Tohoku University
Sendai, Japan

Abstract

The Light Transport Matrix (LTM) is a model of the light ray propagation between a projector and a camera. In case of LTM measurement, sparse estimations are often used. They assume the linearity between the projector and camera intensities. Sparse estimation requires multiple projector pixels to be irradiated together. Since multiple projector pixels are irradiated, the camera captures both the direct and global illumination. When the intensity of the illumination received by a camera pixel is higher than the threshold, camera intensity is clipped to the threshold. The camera intensities can be saturated, even if the LTM elements are not saturated, because of the global illumination. This saturation breaks the assumption of sparse estimation and causes the estimated result to be inaccurate. We propose a new sparse estimation algorithm "Saturation ADMM," which estimates the LTM under conditions in which camera images are saturated because of global illumination. We used numerical simulation and real scene measurement experiments to prove the ability of the proposed method to accurately estimate the LTM under saturated conditions.

1 Introduction

Light transport refers to the behavior of light rays after they are emitted by the light sources until they arrive at the optical sensors. In an active vision system, a projector acts as the light source, and a camera acts as the optical sensor. A system consisting of a projector and a camera is known as a Projector-Camera System and it can be considered as a fundamental component of the active vision system. When the irradiation intensity of the projector and the camera are linear, the light transport between the projector and the camera are described by the Light Transport Matrix (LTM) [11, 15, 19, 20]. The LTM, which can describe all light reflection information, including inter-reflections and subsurface-scatterings for the projector-camera system, is utilized for scene relighting [7, 8, 11, 15, 20], light path understanding (direct/global illumination separation) [1, 2, 12, 13, 14], and 3D measurement [3, 5, 13, 14].

In general, the LTM is a huge matrix because the number of elements is given by the number of combinations between the camera pixels and the projector pixels. Sen et al. [20] proposed an efficient method for the acquisition of the LTM; however, the method cannot measure the LTM efficiently in complex light transport scenes, for example, a scene in which

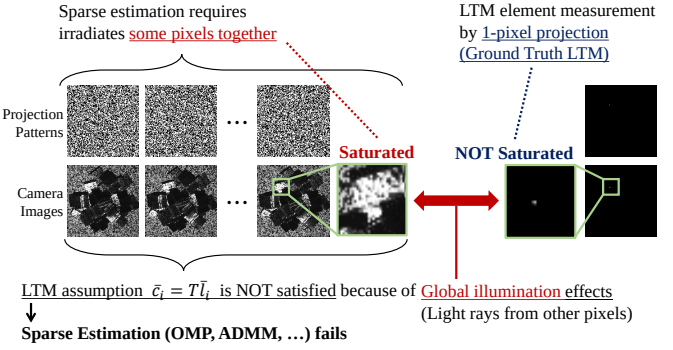

Figure 1: Examples of the projection patterns and camera images. The LTM of the measurement scene includes global illumination, which can saturate the camera pixel intensity for these projection patterns, even if the LTM elements are not actually saturated. This saturation nullifies the LTM assumption that the projector and the camera intensities are linear.

plastic bottles are randomly piled. Thus, various researchers have proposed exploiting the sparseness of LTM by applying sparse sensing techniques to acquire the matrix [3, 8, 16, 17]. Because LTM is sparse in both the spatial domain and the wavelet domain [17], in some studies sparse sensing was applied in the spatial domain [3, 8], whereas in others it was applied in the wavelet domain [16, 17]. Thus, sparse estimation can be utilized to estimate the LTM.

When the sparse sensing method is applied to estimate the LTM, we use some projection patterns as a sensing matrix in the sparse sensing context. Then, the projector irradiates these projection patterns to the measurement scene, and the camera captures reflected lights from the scene as camera images. The camera images act as observed vectors in the sparse sensing context. Finally, sparse sensing methods are used to estimate the LTM as a sparse signal from the sensing matrix and the observed vectors. The sparse sensing method often assumes the observation is given by a linear function; however, because of saturation (blown out highlights) of the camera pixel intensity, the intensity relationship between the projector and the camera can sometimes be nonlinear. This nonlinearity causes the sparse estimation of the LTM to be inaccurate.

We show an example of a saturated condition in Fig. 1. The LTM element is actually non-saturated; however, the camera image pixel intensity is saturated because of global illumination. Global illumination originates from other projector pixels; thus, the more projector pixels are irradiated, the more the possibility of saturation increases[18]. On the other hand, sparse estimation requires us to irradiate some pixels together. These saturated camera images cannot satisfy the LTM assumption of linear intensities; therefore, sparse estimation sometimes fails.

2 LTM Sparse Estimation Problem

This section first describes the projector-camera system in LTM. Because LTM is a very large and sparse matrix, sparse sensing algorithms are applied to measure LTM [3, 8, 16, 17]. We then introduce a formulation for LTM sparse sensing.

2.1 Light Transport Matrix (LTM)

The LTM describes the light transport from the projector pixels to the camera pixels[11, 15, 19, 20]. A projection pattern and a camera image are considered to be vectors, respectively. We define the projection pattern vector and camera image vector as $\boldsymbol{l}$ and $\boldsymbol{c}$, respectively. We denote LTM as L. Here, the light transport is expressed as $\boldsymbol{c} = T\boldsymbol{l}$. When we take some camera image vectors $\boldsymbol{c}_k$, which correspond to projection pattern vectors $\boldsymbol{l}_k$, it can be written as

$$C = TL. \tag{1}$$

with a camera image matrix $C = \begin{bmatrix}\boldsymbol{c}_1 & \boldsymbol{c}_2 & \cdots & \boldsymbol{c}_K\end{bmatrix}$ and a projection pattern matrix $L = \begin{bmatrix}\boldsymbol{l}_1 & \boldsymbol{l}_2 & \cdots & \boldsymbol{l}_K\end{bmatrix}$, where K is the number of projection patterns and captured images. Once we obtain LTM, we can generate a camera image that corresponds to any of the projection patterns by performing easy matrix-vector multiplication. This usage of LTM is known as scene relighting [11, 15, 20].

2.2 Estimation of LTM by Using Sparsity

The naïve way to obtain the LTM is to use 1-pixel projection [3, 5] (described in a study [6] as the impulse response function). However, 1-pixel projection requires as many projection patterns and captured images as the number of projector pixels. Therefore, previous studies [3, 8, 16, 17] proposed sparse estimation of the LTM. The fact that LTM has sparsity in the spatial domain [3, 8] or the wavelet domain [16, 17] means that sparse estimation can be utilized to estimate LTM. In this study we focused on the saturation of the camera pixel intensities in the spatial domain; therefore, sparse estimation formulation in the following discussion is considered to take place in the spatial domain.

Sparse estimation can be used to obtain a sparse vector as an underdetermined problem, which allows the use of fewer observations than the number of dimensions of the estimation vector. The ℓ_1 minimization (LASSO), which is widely used to solve the sparse estimation problem in practice, is defined as

$$\min_{\boldsymbol{x}} \left\{ \|\boldsymbol{x}\|_1 + \frac{1}{2\lambda} \|\boldsymbol{y} - A\boldsymbol{x}\|_2^2 \right\}, \tag{2}$$

where $\lambda > 0$ is the weight of the ℓ_1 regularizer.

We denote the i-th row vector of C and T as $\bar{c}_i$ and $\bar{t}_i$, respectively. Then, Equation (1) can be separated into $\bar{c}_i = \bar{t}_i L$, and finally, it is written as

$$\bar{c}_i^\top = L^\top \bar{t}_i^\top \tag{3}$$

by taking the transpose of both sides. The ℓ_1 minimization can be applied to this form with $\boldsymbol{x} = \bar{t}_i^\top$, $\boldsymbol{y} = \bar{c}_i^\top$, and $\boldsymbol{A} = L^\top$; therefore, we can estimate the LTM by solving

$$\min_{\bar{t}_i} \left\{ \left\| \bar{t}_i^\top \right\|_1 + \frac{1}{2\lambda} \left\| \bar{c}_i^\top - L^\top \bar{t}_i^\top \right\|_2^2 \right\} \tag{4}$$

for all rows.

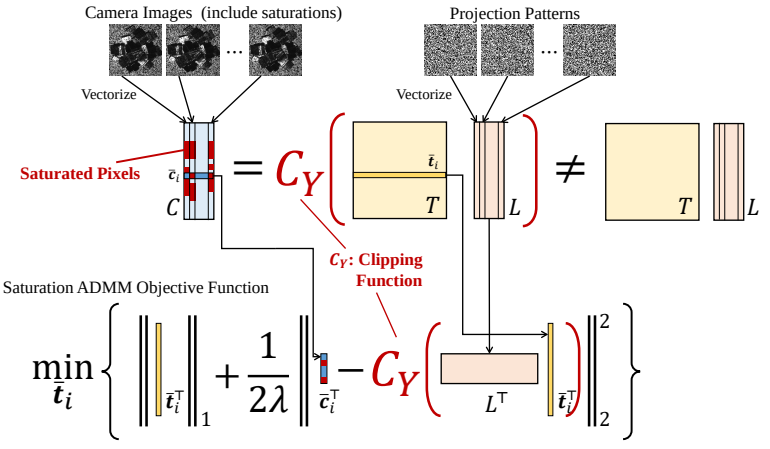

Figure 2: Formulation of the sparse estimation under saturated conditions (Equation (6)). The saturated pixels in the camera image matrix C are shown in red. Then, the Clipping Function is applied for observation as a saturated observation model. This function can be embedded in Equation (4). The saturated pixels differentiate between the linear ($C = TL$) and saturated observation models ($C = C_Y(TL)$)

2.3 Saturated Condition Problem

In practice, saturation of the intensity of a camera image pixel depends on the measurement scene and projection patterns (see Fig. 2). The saturation nullifies the linear relationship between projector intensities and camera intensities. When the intensity of a camera pixel is saturated, the intensity is clipped to the highest intensity. We define the Clipping Function $C_Y(y)$ as

$$C_Y(y) = \begin{cases} y & (y \leq Y) \\ Y & (y > Y) \end{cases}, \tag{5}$$

and we also define $C_Y(\cdot)$ as an application of the Clipping Function to each element of a vector or a matrix. Here, the camera image vector is written as $\bar{c}_i^\top = C_Y\left(L^\top \bar{t}_i^\top\right)$ instead of Equation (3), where Y is the clipping intensity. Therefore, Equation (4) should become

$$\min_{\bar{t}_i} \left\{ \left\| \bar{t}_i^\top \right\|_1 + \frac{1}{2\lambda} \left\| \bar{c}_i^\top - C_Y\left(L^\top \bar{t}_i^\top\right) \right\|_2^2 \right\} \tag{6}$$

under saturated conditions.

3 Saturation ADMM

In this section, we propose a new sparse estimation method "Saturation ADMM," which can solve Equation (6). The Proposed method is based on an application of ADMM (Alternating Direction Method of Multipliers) for ℓ_1 minimization [□]. ADMM can be utilized as an approximate method to solve the ℓ_1 minimization problem. ADMM and Saturation ADMM methods are outlined in Fig. 3.

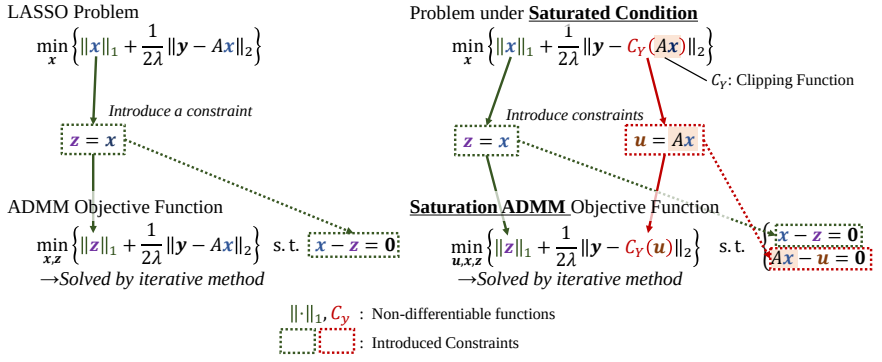

Figure 3: Outline of Saturation ADMM. LASSO (Equation (2)) includes a non-differentiable function $\|\boldsymbol{x}\|_1$. Under saturated conditions, the sparse estimation problem includes two non-differentiable functions $\|\boldsymbol{x}\|_1$ and $C_Y(A\boldsymbol{x})$. We provide an updating rule for the iterative solution of this problem

3.1 Brief Introduction of ADMM

We first briefly introduce an ADMM application for the ℓ_1 minimization problem. The key idea of ADMM is to introduce a new variable $\boldsymbol{z}$ with a constraint $\boldsymbol{x}-\boldsymbol{z}=\boldsymbol{0}$, then Equation (2) is written as

$$\min_{\boldsymbol{x},\boldsymbol{z}} \left\{ \|\boldsymbol{z}\|_1 + \frac{1}{2\lambda}\|\boldsymbol{y}-A\boldsymbol{x}\|_2^2 \right\} \quad \text{s.t.} \quad \boldsymbol{x}-\boldsymbol{z}=\boldsymbol{0}. \tag{7}$$

ADMM utilizes an augmented Lagrangian algorithm for Equation (7). This algorithm introduces a Lagrange multiplier $\boldsymbol{h}$ and a penalty coefficient $\mu > 0$. Here, the objective function is given by

$$L(\boldsymbol{x},\boldsymbol{z};\boldsymbol{h}) = \|\boldsymbol{z}\|_1 + \frac{1}{2\lambda}\|\boldsymbol{y}-A\boldsymbol{x}\|_2^2 + \boldsymbol{h}^\top(\boldsymbol{x}-\boldsymbol{z}) + \frac{\mu}{2}\|\boldsymbol{x}-\boldsymbol{z}\|_2^2. \tag{8}$$

In this function, ADMM updates $\boldsymbol{h}$, $\boldsymbol{x}$, and $\boldsymbol{z}$, alternately.

The Lagrange multiplier $\boldsymbol{h}$ is updated by

$$\boldsymbol{h} \leftarrow \boldsymbol{h} + \mu(\boldsymbol{x}-\boldsymbol{z}). \tag{9}$$

Updating rule of $\boldsymbol{x}$ is given in the quadratic form, which is solved as

$$\boldsymbol{x} \leftarrow \left(\frac{1}{\lambda}A^\top A + \mu I\right)^\dagger \left(\frac{1}{\lambda}A^\top \boldsymbol{y} + \mu\boldsymbol{z} - \boldsymbol{h}\right), \tag{10}$$

where † is the pseudo-inverse, and I is the identity matrix. Updating rule of $\boldsymbol{z}$ is given by

$$\arg\min_{\boldsymbol{z}} \left\{ \|\boldsymbol{z}\|_1 + \frac{\mu}{2}\left\|\boldsymbol{x}-\boldsymbol{z}+\frac{1}{\mu}\boldsymbol{h}\right\|_2^2 \right\} = \sum_i \arg\min_{z_i} \left\{ |z_i| + \frac{\mu}{2}\left(x_i - z_i + \frac{1}{\mu}h_i\right)^2 \right\}, \tag{11}$$

where z_i denotes the i-th element of $\boldsymbol{z}$. By this deformation, Equation (11) can be solved element-wise with condition analysis. We denote the i-th element of $\boldsymbol{x}$ and $\boldsymbol{h}$ as x_i and h_i,

respectively. Here, the Soft Thresholding Function $S_\lambda(y)$ is defined by

$$S_\lambda(q) = \begin{cases} q-\lambda & (\lambda \le x) \\ 0 & (-\lambda \le q < \lambda) \\ q+\lambda & (q \le -\lambda) \end{cases}, \tag{12}$$

and $S_\lambda(\boldsymbol{q})$ is also defined as applying the Soft Thresholding Function for each element of $\boldsymbol{q}$. Then, $\boldsymbol{z}$ is given by

$$\boldsymbol{z} \leftarrow S_{\frac{1}{\mu}}\left(\boldsymbol{x} + \frac{1}{\mu}\boldsymbol{h}\right). \tag{13}$$

3.2 Saturation ADMM Algorithm

When estimating the LTM, we need to solve Equation (6) instead of Equation (2) because the camera pixel intensities are saturated in practice. We assume the observed value of y_i is smaller than Y ($y_i \le Y$), where y_i denotes the i-th element of $\boldsymbol{y}$. We introduce a new variable $\boldsymbol{u}$ and a new constraint $A\boldsymbol{x} - \boldsymbol{u} = \boldsymbol{0}$; then the objective function is expressed as

$$\min_{\boldsymbol{u},\boldsymbol{x},\boldsymbol{z}} \left\{ \|\boldsymbol{z}\|_1 + \frac{1}{2\lambda}\|\boldsymbol{y} - C_Y(\boldsymbol{u})\|_2^2 \right\} \quad \text{s.t.} \quad \begin{cases} \boldsymbol{x} - \boldsymbol{z} = \boldsymbol{0} \\ A\boldsymbol{x} - \boldsymbol{u} = \boldsymbol{0} \end{cases}. \tag{14}$$

We define a new Lagrange multiplier $\boldsymbol{g}$ and penalty coefficient $\nu > 0$. Combining the new constraint, Lagrange multiplier, and penalty coefficient with Equation (8), the new objective function is

$$L(\boldsymbol{u},\boldsymbol{x},\boldsymbol{z};\boldsymbol{h},\boldsymbol{g}) \tag{15}$$

$$= \|\boldsymbol{z}\|_1 + \frac{1}{2\lambda}\|\boldsymbol{y} - C_Y(\boldsymbol{u})\|_2^2 + \boldsymbol{h}^\top(\boldsymbol{x}-\boldsymbol{z}) + \frac{\mu}{2}\|\boldsymbol{x}-\boldsymbol{z}\|_2^2 + \boldsymbol{g}^\top(A\boldsymbol{x}-\boldsymbol{u}) + \frac{\nu}{2}\|A\boldsymbol{x}-\boldsymbol{u}\|_2^2. \tag{16}$$

We update $\boldsymbol{h}$, $\boldsymbol{g}$, $\boldsymbol{u}$, $\boldsymbol{x}$, and $\boldsymbol{z}$, alternately.

According to ADMM, the respective Lagrange multipliers $\boldsymbol{h}$, $\boldsymbol{g}$ are updated by $\boldsymbol{h} \leftarrow \boldsymbol{h} + \mu(\boldsymbol{x}-\boldsymbol{z})$, $\boldsymbol{g} \leftarrow \boldsymbol{g} + \nu(A\boldsymbol{x}-\boldsymbol{u})$, respectively. When $\boldsymbol{x}$, $\boldsymbol{z}$, or $\boldsymbol{u}$ is updated, the other variables are considered to remain constant.

In the step in which $\boldsymbol{x}$ is updated, $\boldsymbol{x}$ is still in the quadratic form; thus, it can be solved as

$$\boldsymbol{x} \leftarrow \left(\nu A^\top A + \mu I\right)^\dagger \left(A^\top(\nu\boldsymbol{u} - \boldsymbol{g}) + \mu\boldsymbol{z} - \boldsymbol{h}\right). \tag{17}$$

In the step in which $\boldsymbol{z}$ is updated, $\boldsymbol{z}$ is updated by the same equation used in ADMM; thus, the updating rule is given by Equation (13).

In the step in which $\boldsymbol{u}$ is updated, we define a vector $\boldsymbol{v}$ as $\boldsymbol{v} = A\boldsymbol{x} + \frac{1}{\nu}\boldsymbol{g}$; then, the rule to update $\boldsymbol{u}$ is written as

$$\arg\min_{\boldsymbol{u}} \left\{ \|\boldsymbol{y} - C_Y(\boldsymbol{u})\|_2^2 + \lambda\nu\|\boldsymbol{v}-\boldsymbol{u}\|_2^2 \right\} = \sum_i \left\{ \arg\min_{u_i} (y_i - C_Y(u_i))^2 + \lambda\nu(v_i - u_i)^2 \right\}, \tag{18}$$

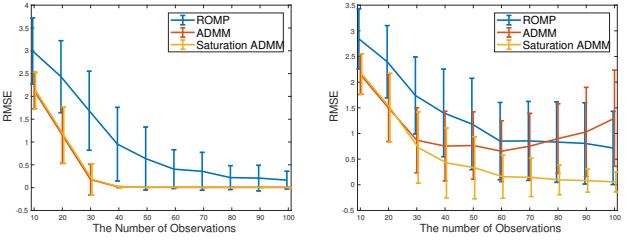

(a) Non-saturated condition (b) Saturated condition

Figure 4: Root Mean Square Error (RMSE) of sparse estimation in numerical simulation. Results of (a) non-saturated and (b) saturated condition. The problem includes random values; thus, the simulation was iterated 100 times. The figure shows the mean and standard deviation values of the RMSE.

where u_i and v_i are the i-th element of $\boldsymbol{u}$ and the i-th element of $\boldsymbol{v}$, respectively. According to Equation (18), u_i is calculated element-wise with condition analysis as

$$\arg\min_{u_i}\left\{(y_i - C_Y(u_i))^2 + \lambda\nu\,(v_i-u_i)^2\right\} = \begin{cases} \dfrac{y_i+\lambda\nu v_i}{1+\lambda\nu} & \left(v_i \le y_i + \sqrt{1+\dfrac{1}{\lambda\nu}}\,(Y-y_i)\right) \\ v_i & \left(v_i > y_i + \sqrt{1+\dfrac{1}{\lambda\nu}}\,(Y-y_i)\right) \end{cases} \tag{19}$$

Here, we define a function $D(x;\theta,\xi)$ as

$$D(x;\theta,\xi) = \begin{cases} \xi & (x \le \theta) \\ x & (x > \theta) \end{cases}, \tag{20}$$

and we consider the same extension of $D(x_i;\theta_i,\xi_i)$ as the Soft Thresholding Function and the Clipping Function for a vector, then Equation (19) is given by

$$\boldsymbol{u} \leftarrow D\left(\boldsymbol{v}; \boldsymbol{y} + \sqrt{1+\frac{1}{\lambda\nu}}\,(Y\mathbf{1}-\boldsymbol{y}), \frac{1}{1+\lambda\nu}\boldsymbol{y} + \frac{\lambda\nu}{1+\lambda\nu}\boldsymbol{v}\right), \tag{21}$$

where $\mathbf{1}$ is a vector of which all elements are 1.

4 Experiment

In this experiment section, we prove that the proposed method can be applied to the sparse estimation of LTM by numerical simulation, comparing estimation errors, and scene relighting.

4.1 Numerical Simulation

We first prove that Saturation ADMM can solve both of the ℓ_1 minimization problem and saturated problem by numerical simulations. We set the number of dimensions of the estimation

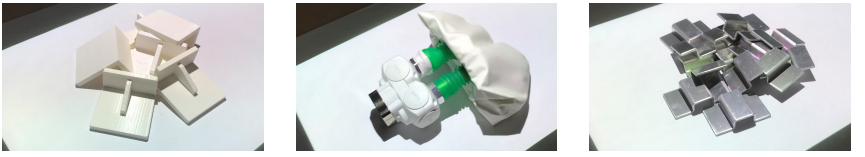

(a) L Objects (b) Gripper (c) Metallic Objects

Figure 5: Measurement scenes. (a) L-shaped white objects are randomly located in the scene. (b) A robot hand gripper is located on a sheet of paper. (c) Metallic industrial objects are randomly located on a sheet of paper.

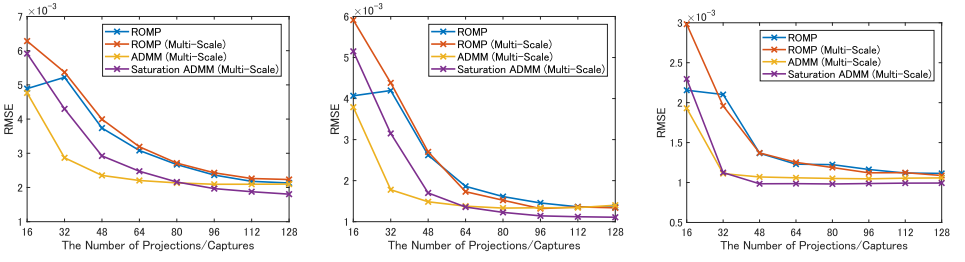

(a) L Objects (b) Gripper (c) Metallic Objects

Figure 6: RMSE between 1-pixel projection responses and estimated LTMs. The 1-pixel projection responses are captured only for the 256 pixels out of a total of 16,384 projector pixels as uniformly sampled points, because measuring the 1-pixel projection responses for all projector pixels is excessively time consuming.

sparse vector $\boldsymbol{x}$ as 100, and it has $10[\%]$ non-zero elements given by uniform distribution in $[0,1]$. We also set the observation matrix A as random values by uniform distribution in $[0,1]$. Under non-saturation conditions, the observed vector is calculated by $\boldsymbol{y} = A\boldsymbol{x}$, and under saturated conditions, we clip the observed vector as $\boldsymbol{y} = C_3(A\boldsymbol{x})$. The number of observations (dimension of $\boldsymbol{y}$) is controlled from 10 to 100 within increments of 10. We compared our results with those obtained with ROMP (Regularized Orthogonal Matching Pursuit) [10], which is used in studies [7, 8], and ADMM which is used in studies [3].

The results of the numerical simulation are shown in Fig. 4, in which the RMSE between the estimated $\boldsymbol{x}$ and the ground truth. Under non-saturated conditions, ADMM and Saturation ADMM outperform ROMP. The curves of the RMSE of ADMM and Saturation ADMM are almost the same. In addition, Saturated ADMM can estimate under saturated conditions. On the other hand, the RMSE of ADMM does not converge under saturated conditions, because ADMM assumes $\boldsymbol{y} = A\boldsymbol{x}$, but the observation is saturated under this condition.

4.2 Experiments in real scenes

Second, we attempted to measure the LTM on four real scenes, as shown in Fig. 5. Our projector-camera system is fixed on top, and they are calibrated to be over-wrap their projection area and capture area by using homography matrices. We set the resolution of both the projector and the camera as 128×128. The projection patterns are the Bernoulli binary patterns that are used in a study [17]. We apply ROMP, ADMM, and Saturated ADMM to estimate the LTM. We also utilize the multi-scale estimation technique [4] to accelerate

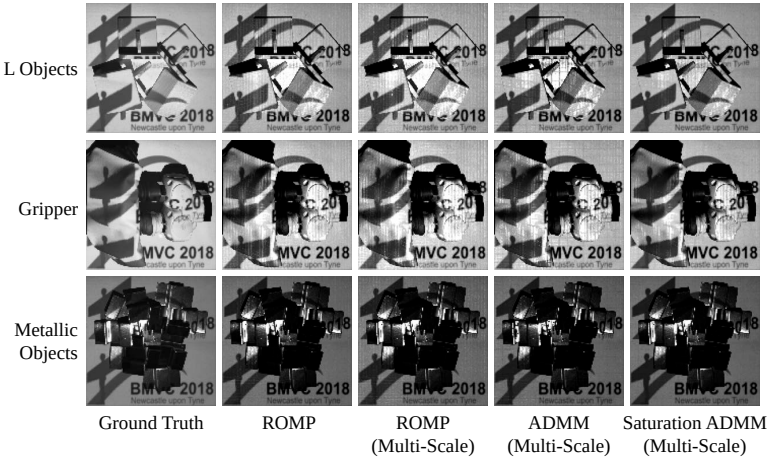

Figure 7: Simulated camera images via scene relighting (BMVC Logo, on L Objects, Gripper, and Metallic Objects). Ground Truth is a camera image with the pattern projection, and the others are scene relighting results by LTMs.

the computation and obtain high-resolution results. The ground truth is measured by using 1-pixel projection. We sampled 256 points uniformly out of a total of 16,384 projector pixels.

The results are shown in Fig. 6. ROMP and ROMP with multi-scale converges to a higher RMSE than the other methods, in the all scenes. With a small number of projections/captures (< 64), ADMM with Multi-Scale obtains the lowest RMSE; however, ADMM with Multi-Scale RMSE converges to a higher RMSE in Saturation ADMM with Multi-Scale. Therefore, for real scene sensing, the proposed method ultimately estimates the LTM with the lowest RMSE.

4.3 Relighting

We attempted to utilize the estimated LTMs to perform scene relighting [8, 20]. We used the BMVC Logo image as a projection pattern for scene relighting. The relighting results are shown in Fig. 7. ADMM with Multi-Scale always displays a grid on the relighted camera images. These grids occur because nonlinear response (mainly saturation) sometimes occurs on the grids. Saturation ADMM estimates LTM well under these nonlinear responses.

5 Conclusion

In this paper, we proposed a new LTM estimation method. We focused on the saturation of camera image pixels, which often occurs in real sensing and affects sparse estimation. We then formulated the saturation in the ℓ_1 minimization problem, and proposed a method named "Saturation ADMM," which is based on ADMM. Finally, we applied the proposed method for LTM estimation. The numerical simulation experiment showed that Saturation ADMM can converge to a lower RMSE than the other sparse estimation methods under saturated conditions. In the real scenes, Saturation ADMM performed better than the others.

References

[1] Jiamin Bai, Manmohan Chandraker, Tian-Tsong Ng, and Ravi Ramamoorthi. A Dual Theory of Inverse and Forward Light Transport. In *Proceedings of European Conference on Computer Vision*, pages 1–8, 2010.

[2] Stephen Boyd, Neal Parikh, Eric Chu, Borja Peleato, and Jonathan Eckstein. Distributed Optimization and Statistical Learning via the Alternating Direction Method of Multipliers. *Foundation and Trends in Machine Learning*, 3(1):1–122, 2011.

[3] Naoya Chiba and Koichi Hashimoto. 3D Measurement by Estimating Homogeneous Light Transport (HLT) Matrix. In *Proceedings of IEEE International Conference on Mechatronics and Automation*, pages 1763–1768, 2017.

[4] Naoya Chiba and Koichi Hashimoto. Ultra-Fast Multi-Scale Shape Estimation of Light Transport Matrix for Complex Light Reflection Objects. In *Proceedings of IEEE International Conference on Robotics and Automation*, 2018.

[5] Naoya Chiba, Shogo Arai, and Koichi Hashimoto. Feedback Projection for 3D Measurements Under Complex Lighting Conditions. In *Proceedings of American Control Conference*, pages 4649–4656, 2017.

[6] Michael Goesele, Hendrik P. A. Lensch, Jochen Lang, Christian Fuchs, and Hans-Peter Seidel. DISCO: Acquisition of Translucent Objects. *ACM Transactions on Graphics*, 23(3):835–844, 2004.

[7] Isao Miyagawa and Tetsuya Kinebuchi. Compressive Inverse Light Transport for Radiometric Compensation in Projection-based Displays. *ITE Transactions on Media Technology and Applications*, 5(3):96–109, 2017.

[8] Isao Miyagawa, Yukinobu Taniguchi, and Tetsuya Kinebuchi. Radiometric Compensation Using Color-Mixing Matrix Reformed from Light Transport Matrix. *ITE Transactions on Media Technology and Applications*, 4(2):155–168, 2016.

[9] Osamu Nasu, Shinsaku Hiura, and Kosuke Sato. Analysis of Light Transport based on the Separation of Direct and Indirect Components. In *Proceedings of IEEE Conference on Computer Vision and Pattern Recognition*, pages 1–2, 2007.

[10] Deanna Needell and Roman Vershynin. Signal Recovery From Incomplete and Inaccurate Measurements Via Regularized Orthogonal Matching Pursuit. *IEEE Journal of Selected Topics in Signal Processing*, 4(2):310–316, 2010.

[11] Ren Ng, Ravi Ramamoorthi, and Pat Hanrahan. All-frequency Shadows Using Nonlinear Wavelet Lighting Approximation. *ACM Transactions on Graphics*, 22(3):376–381, 2003.

[12] Matthew O'Toole, Ramesh Raskar, and Kiriakos N. Kutulakos. Primal-dual Coding to Probe Light Transport. *ACM Transactions on Graphics*, 31(4):39:1–39:11, 2012.

[13] Matthew O'Toole, John Mather, and Kiriakos N. Kutulakos. 3D Shape and Indirect Appearance by Structured Light Transport. In *Proceedings of Conference on Computer Vision and Pattern Recognition*, pages 3246–3253, 2014.

[14] Matthew O'Toole, John Mather, and Kiriakos N. Kutulakos. 3D Shape and Indirect Appearance by Structured Light Transport. *IEEE Transactions on Pattern Analysis and Machine Intelligence*, 38(7):1298–1312, 2016.

[15] Pieter Peers and Philip Dutré. Wavelet Environment Matting. In *Proceedings of the 14th Eurographics Workshop on Rendering*, pages 157–166, 2003.

[16] Pieter Peers, Dhruv K. Mahajan, Bruce Lamond, Abhijeet Ghosh, Wojciech Matusik, Ravi Ramamoorthi, and Paul Debevec. Compressive Light Transport Sensing. *ACM Transactions on Graphics*, 28(1):3:1–3:18, 2009.

[17] Pradeep Sen and Soheil Darabi. Compressive Dual Photography. *Computer Graphics Forum*, 28(2):609–618, 2009.

[18] Yoav Y. Schechner, Shree K. Nayar, and Peter N. Belhumeur. A theory of multiplexed illumination. In *Proceedings the 9th IEEE International Conference on Computer Vision*, volume 2, pages 808–815 vol.2, 2003.

[19] Steven M. Seitz, Yasuyuki Matsushita, and Kiriakos N. Kutulakos. A Theory of Inverse Light Transport. In *Proceedings of IEEE International Conference on Computer Vision*, pages 1440–1447, 2005.

[20] Pradeep Sen, Billy Chen, Gaurav Garg, Stephen R. Marschner, Mark Horowitz, Marc Levoy, and Hendrik P. A. Lensch. Dual Photography. *ACM Transactions on Graphics*, 24(3):745–755, 2005.